



UNIVERSITY OF LEEDS

This is a repository copy of *Ecofriendly alkali metal cations diffusion improves fabrication of mixed-phase titania polymorphs on fixed substrate by chemical vapor deposition (CVD) for photocatalytic degradation of azo dye.*

White Rose Research Online URL for this paper:

<https://eprints.whiterose.ac.uk/204998/>

Version: Accepted Version

Article:

Chankhunthod, N., Junploy, P. orcid.org/0000-0002-0820-3203, Suthirakun, S. et al. (10 more authors) (2023) Ecofriendly alkali metal cations diffusion improves fabrication of mixed-phase titania polymorphs on fixed substrate by chemical vapor deposition (CVD) for photocatalytic degradation of azo dye. *Environmental Research*, 239 (Part 2). 117347. ISSN 0013-9351

<https://doi.org/10.1016/j.envres.2023.117347>

© 2023, Elsevier. This manuscript version is made available under the CC-BY-NC-ND 4.0 license <http://creativecommons.org/licenses/by-nc-nd/4.0/>.

Reuse

This article is distributed under the terms of the Creative Commons Attribution-NonCommercial-NoDerivs (CC BY-NC-ND) licence. This licence only allows you to download this work and share it with others as long as you credit the authors, but you can't change the article in any way or use it commercially. More information and the full terms of the licence here: <https://creativecommons.org/licenses/>

Takedown

If you consider content in White Rose Research Online to be in breach of UK law, please notify us by emailing eprints@whiterose.ac.uk including the URL of the record and the reason for the withdrawal request.



eprints@whiterose.ac.uk
<https://eprints.whiterose.ac.uk/>

Ecofriendly alkali metal cations diffusion improves fabrication of mixed-phase titania polymorphs on fixed substrate by chemical vapor deposition (CVD) for photocatalytic degradation of azo dye

Navadecho Chankhunthod ^{a,j,1}, Patcharanan Junploy ^{b,1}, Suwit Suthirakun ^c, Lappawat Ngamwongwa ^d, Chitsanupong Phromma ^e, Nantawat Ruchusartsawat ^e, Adisak Siyasukh ^e, Pattama Yanu ^f, Pimluck Kijjanapanich ^g, Saranphong Yimklan ^h, Apinpus Rujiwatra ^h, Rik Drummond-Brydson ^{i,*}, Yothin Chimupala ^{e,k,*}

^a Department of Physics, Faculty of Science, Khon Kaen University, Khon Kaen, 40002, Thailand.

^b Department of Chemistry, Faculty of Science and Technology, Chiang Mai Rajabhat University, Chiang Mai, Thailand.

^c School of Chemistry, Institute of Science, Suranaree University of Technology, Nakhon Ratchasima 30000, Thailand.

^d School of Physics, Institute of Science, Suranaree University of Technology, Nakhon Ratchasima 30000, Thailand.

^e Department of Industrial Chemistry, Faculty of Science, Chiang Mai University, Chiang Mai, 50200, Thailand.

^f Chiang Mai University Demonstration School, Faculty of Education, Chiang Mai University, Chiang Mai 50200, Thailand.

^g Department of Environmental Engineering, Faculty of Engineering, Chiang Mai University, Chiang Mai 50200, Thailand

^h Department of Chemistry, Faculty of Science, Chiang Mai University, Chiang Mai, 50200, Thailand.

ⁱ School of Chemical and Process Engineering, University of Leeds, Leeds, LS2 9JT, United Kingdom.

^j Institute of Nanomaterials Research and Innovation for Energy (IN-RIE), NANOTECH-KKU RNN on Nanomaterials Research and Innovation for Energy, Khon Kaen University, 40002, Thailand.

^k Center of Excellence in Materials Science and Technology, Chiang Mai University, Chiang Mai 50200, Thailand.

* Corresponding author. Department of Industrial Chemistry, Faculty of Science, Chiang Mai University, Chiang Mai, 50200, Thailand.

* Corresponding author.

E-mail addresses : R.M.Drummond-Brydson@leeds.ac.uk (R. Drummond-Brydson), yothin.chimupala @cmu.ac.th (Y. Chimupala).

¹ Co-first Authors.

ABSTRACT

Controlling the nanoscale synthesis of semiconductor TiO_2 on a fixed substrate has fascinated the curiosity of academics for decades. Synthesis development is required to give an easy-to-control technique and parameters for TiO_2 manufacture, leading to advancements in prospective applications such as photocatalysts. This study, mixed-phase $\text{TiO}_2(\text{B})$ /other titania thin films were synthesized on a fused quartz substrate utilizing a modified CVD involving alkali-metal ions (Li^+ , Na^+ , and K^+) solution pre-treatment. It was discovered that different cations promote dramatically varied phases and compositions of thin films. The films had a columnar structure with agglomerated irregular-shaped particles with a mean thickness of 800-2000 nm. Na^+ ions can promote $\text{TiO}_2(\text{B})$ more effectively than K^+ ions, however Li^+ ions cannot synthesize $\text{TiO}_2(\text{B})$. The amounts of $\text{TiO}_2(\text{B})$ in thin films increase with increasing alkali metal (K^+ and Na^+) concentration. According to experimental and DFT calculations, the hypothesized $\text{TiO}_2(\text{B})$ production mechanism happened via the meta-stable intermediate alkaline titanate transformation caused by alkali-metal ion diffusion. The mixed phase of $\text{TiO}_2(\text{B})$ and anatase TiO_2 on the fixed substrate ($1 \times 1 \text{ cm}^2$) obtained from Na^+ pre-treated procedures showed significant photocatalytic activity for the degradation of methylene blue. $\text{K}_2\text{Ti}_6\text{O}_{12}$, Li_2TiO_3 , Rutile TiO_2 , and Brookite TiO_2 phase formations produced by K^+ and Li^+ pretreatment are low activity photocatalysts. Photocatalytic activities were more prevalent in NaOH pre-treated samples (59.1 % dye degradation) than in LiOH and KOH pre-treated samples (49.6% and 34.2%, respectively). This revealed that our developed CVD might generate good photocatalytic thin films of mixed-phase $\text{TiO}_2(\text{B})$ /anatase TiO_2 on any substrate, accelerating progress in future applications.

KEYWORDS: photocatalytic TiO_2 , phase formation, alkali metal cation, titania/titanate thin films, chemical vapor deposition, dye degradation

1. Introduction

Titania or titanium dioxide (TiO_2) is an interesting semiconductor that has received significant attention over the last decade. It has been proposed as a promising candidate in many fields of research and applications, such as photovoltaics (Bai et al., 2014), pigment (El-Sherbiny et al., 2014), optical coating (Jayasinghe et al., 2012), storage devices (Zheng et al., 2023), and photocatalysis (Schneider et al., 2014; Setvin et al., 2017). TiO_2 exhibits high oxidative ability, is cost-effective, environmentally friendly, safe, and has physical and chemical stability (Wan et al., 2015) and is considered the most promising photocatalytic material for solving energy-related and environmental issues (Ma et al., 2014). Most TiO_2 nanostructures, such as nanoparticles, nanotubes, and nanowires, have been extensively studied recently due to their structural advantage representing a very high surface area to volume ratio (Chen and Selloni, 2014). Two-dimensional (2D) thin films have many advantages among these nanostructures. The 2D thin films are easy to control parameters such as film thickness and surface area, which govern their behaviors and properties of the films. This allows more interfaces of TiO_2 to react with pollutant elements from water or air, leading to an increase in photocatalytic activity.

Various polymorphs of TiO_2 , including anatase, rutile, brookite, and $\text{TiO}_2(\text{B})$ have been developed as effective photocatalysts (Schneider et al., 2014). Among these crystallographically unique structures, the anatase exhibits the best photocatalytic activity over rutile, brookite, and $\text{TiO}_2(\text{B})$. However, mixed phases of anatase/rutile or anatase/ $\text{TiO}_2(\text{B})$ have been reported with better photocatalytic activity than pure anatase (Carmichael et al., 2013; Mohamed et al., 2012). In addition, combining two different titania phases affects the charge transfer process between the different phases, possibly reducing photo-generated electron-holes recombination, thus enhancing the photocatalytic activity (Bai et al., 2009; Huang et al., 2012; Yang et al., 2009; Zheng et al., 2009).

Various synthesis methods of TiO_2 thin films, including physical vapor deposition (PVD), such as evaporation and sputtering, sol-gel method, and chemical vapor deposition (CVD) (Y. Chimupala et al.,

2014; Djaoued et al., 2002; Guillén et al., 2014; Masuda et al., 2009; Pyun et al., 2010) have been continuously developed to promote nanoscale thin films with excellent performance. The CVD method is a low-cost and straightforward deposition with an uncomplicated process to provide excellent coverage step of nanofilm layers. Additionally, this technique can directly deposit thin film onto many substrates and/or electrodes, which could be applied in other promising applications such as Li-ion battery applications. However, the drawback of using mixed titania polymorph is the difficulty of the preparation method, especially in large-scale production. However, as we mentioned above, this CVD method is capable for preparing the mixed phase titania thin film by modified alkali metal cations e.g., Na⁺ during the deposition process.

According to our previous work in 2014, Chimupala et al.(Chimupala et al., 2014a,b) first reported the success of mixed-phase of anatase and TiO₂(B) preparation onto soda-lime glass substrates using low-pressure CVD (LPCVD). The proposed mechanism of TiO₂(B) formation occurred during the deposition process because of Na⁺ ions diffusion from the glass into the titania structures. This discovery could lead to a promising synthesis route for producing pure phase or mixed phases of nanostructured TiO₂ thin films on substrates with high photocatalytic activity. Moreover, most TiO₂(B) nanostructures were usually synthesized from the hydrothermal method (Chimupala and Drummond-Brydson, 2018) and sol-gel route engaging with alkali-metal cations, requiring multi-step synthesis and long reaction time. One-step synthesis, such as the CVD process, is required to provide an advance in TiO₂(B) synthesis to address these issues. In 2016, a pre-treatment method involving spraying an NaOH solution onto several different substrates was applied in conjunction with the LCVD process to promote the TiO₂(B) phase in the thin film products (Chimupala et al., 2016). Regarding the practical application, an immobilized titania thin film on rigid substrates is a necessary form of these photocatalysts to be employed. Therefore, the preparing mixed-phase TiO₂(B)/other titania polymorph thin films by pre-treatment modified CVD method with a different type of alkali-metal ions is the main objective of this research, and the effect of alkaline ions must be considered for maximizing phase compositions for promoting the titania thin films on substrates for the potential applications.

Here in, the specific objectives of this work as points (i) to prepare mixed nanophase TiO₂(B)/other titania thin films by modified CVD involving an alkaline ion solution pre-treatment on substrate surfaces, (ii) to examine the effects of alkali metal ions, including lithium (Li⁺), sodium (Na⁺), and potassium (K⁺) on the TiO₂/titanates phase formation, (iii) to investigate the transformation mechanisms during the migration of alkali metal ions (Li⁺, Na⁺ and K⁺) through the titania structure by experimental results and DFT calculations, and (iv) to study the photocatalytic activity of the synthesized titania thin film for wastewater treatment applications. To our knowledge, a substrate pre-treatment involving different alkali metal ions (Li⁺, Na⁺, and K⁺) solution in the fabrication of mixed titania/TiO₂(B) thin film using CVD was first introduced. This demonstrated the effectiveness of the proposed universal alkaline ions pre-treatment method as a novel synthesis method for promoting pure/mixed TiO₂ thin films on any substrate with a potential for promising ecofriendly applications such as preparing mixed titania/TiO₂(B) thin film on electrode as a novel active anode material in Li-ion batteries (Pimta, et al., 2023).

2. Materials and Methods

2.1 Materials

All chemical reagents used in this study were analytical grade and used without further purification. The 97% purity of titanium tetra-isopropoxide (TTIP) was purchased from Sigma-Aldrich and used as the precursor of titanium source for promoting TiO₂ nanophase. Lithium hydroxide (LiOH, 98%) and potassium hydroxide (KOH, 90%) were ordered from Sigma-Aldrich. Sodium hydroxide (NaOH, 97.5%) was purchased from Scientific Laboratory supplies. Hydrochloric acid (HCl) was purchased from RCI Labscan limited. Deionized water was used to prepare the alkaline solution for the substrate pre-treatment process. Fused quartz was used as substrate.

2.2 Substrate pre-treatment of the fused quartz substrate

The modified spraying method was used to provide alkali-metal-cation layers onto the surface of the substrate. In brief, 0.5 mL of alkaline solution such as NaOH solution (0.25 M, 0.50 M, 1.0 M, and 2.0 M) was gently sprayed onto 10 mm × 10 mm × 3 mm (width × length × thickness) fused quartz substrate which was set at 15 cm away from the spraying source. The modified substrate was labeled as 0.25M_X, 0.50M_X, 1.0M_X, and 2.0M_X (where X = Li, Na, K), respectively, and left dry at 50 °C for 12 h before the CVD process. Finally, the alkaline-coated substrates were placed into the quartz tube at a center position before thin film deposition. In order to study the effect of alkaline metal ions for introducing TiO₂ phase formation, other alkali metal hydroxide solutions, including LiOH and KOH with similar concentrations, were also prepared in the substrate pre-treatment process to obtain the modified alkaline ion substrates.

2.3 TiO₂ thin-film deposition using CVD

Polymorphs of TiO₂, including TiO₂(B) and other alkaline-titanate thin films, were fabricated by a modified CVD following the previous synthesis method (Chimupala et al., 2016). In brief, 5.0 mL of TTIP precursor was injected into a bubbling chamber and settled in an oil bath at approximately 90 °C. Next, the quartz tube and the alkaline-coated substrates were pre-heated in the furnace up to the 600 °C reaction temperature for 30 min. Then, 1000 mL/min N₂ flow was used to carry the TTIP vapor into the reaction chamber for 15 min operating at atmospheric pressure. After that, the reaction stopped and began slowly cooling to room temperature.

2.4 Photocatalytic reduction of methylene blue

Photocatalytic activities of the as-prepared TiO₂ thin films were performed in terms of methylene blue (MB) degradation by an advanced oxidation process. In detail, the deposited TiO₂/titania thin films were placed on the bottom of a 15 mL cylindrical Pyrex vessel. The 5 × 10⁻⁶ M of MB solution was filled into the vessels. Four 18 W tubular black light lamps which irradiated UV-A wavelength region (315-400 nm)

were used to initiate the photocatalytic reaction. After keeping the reaction vessel in the dark box for 30 minutes, the solution was irradiated with UV light for 6 hours. The degraded MB solution was then transferred to UV-Quartz cuvette for the degradation investigation by UV-Visible spectrometry.

2.5 Materials characterization

X-ray diffraction (XRD) patterns of all samples were characterized by a Phillips X'Pert MPD diffractometer, United Kingdom working with an X-ray source from Cu K α irradiation ($\lambda = 1.545 \text{ \AA}$). It was operated at room temperature with a 2θ during X-ray scanning with a scan step of 0.02° and a scan speed of $20^\circ/\text{min}$. After that, All XRD patterns were identified phases and crystallographic structures using X'pert high score plus software with the diffraction database (JCPDS card). The morphologies and elemental compositions of all TiO₂ products were studied in both plan view and cross-section by using scanning electron microscopy (Carl Zeiss LEO 1530 Gemini FE-SEM, Germany) and FE-Scanning Electron Microscope: JSM 6335 F, Japan). The SEM was fitted with an energy-dispersive X-ray (EDX) detector (Oxford Instruments). Images were recorded and processed using ImageJ software. Photocatalytic activity of synthesized TiO₂/Titania thin films was investigated via degradation of methylene blue after UV-light irradiation. The degraded MB solution has measured the degradation using UV-vis spectroscopy (Lambda 25 Perkin Elmer, United States) using the absorbance intensity at 664 nm.

2.6 Computational detail

A computational model was employed to understand better the TiO₂(B) formation mechanism resulting from different types of alkaline ions. The details of computational simulation for the diffusion of the alkaline atom in alkaline titanates were described as follows. In brief, the ground state structures and energies of the alkaline hexa-titanates (A₂Ti₆O₁₃), where A = Li, Na, and K, were obtained from the spin-polarized density functional theory (DFT) implemented in Vienna Ab-initio Simulation Package (VASP) (Kresse and Furthmüller, 1996a, 1996b; Kresse and Hafner, 1993; Samsudin et al., 2015). The exchange-correlation term was treated using the Perdew-Burke-Ernzerhof functional within the generalized gradient

approximation (Perdew et al., 1996). The projector augmented wave pseudopotential is treated to describe the interaction between the core and valence electrons (Blöchl, 1994; Joubert, 1999). The considered valence electrons Li $1s2s$, O $2s2p$, Na $2p3s$, K $3p4s$, and Ti $3p3d4s$ wavefunctions were expanded in the plane wave basis with a cut-off energy of 500 eV. In the self-consistent electronic field, the tolerance of total energy difference was set to 10^{-6} eV. In addition, models of monoclinic $A_2Ti_6O_{13}$ are fully optimized until the atomic force is no greater than 0.02 eV/Å, using the first Brillouin zone sampling with k-mesh of $2 \times 7 \times 3$ by the Monkhorst-Pack scheme (Monkhorst and Pack, 1976). The optimized cell parameters are shown in Table S1.

To investigate the diffusion of the alkali metal atom (A) in $A_2Ti_6O_{13}$, we modelled the movement of an A vacancy in the system, equivalent to atom A diffusing in the opposite direction. In this case, the supercell of $1 \times 3 \times 1$, including 126 atoms, was used to lessen the interaction between vacancies, and the associated sampling k-points of $2 \times 2 \times 2$ were also used. To study the kinetics of the diffusion, we employed Nudge Elastic Band (CI-NEB) method (Henkelman et al., 2000) as implemented in VASP to find the minimum energy pathway as well as the corresponding energy barrier of the diffusion. In total, five images between two endpoints were optimized until they reached the convergence criterion for the force along the NEB path less than 0.05 eV/Å.

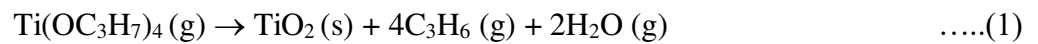
3. RESULTS AND DISCUSSION

3.1 The influences of Na^+ ion on the formation of titania thin films.

Generally, the controlled TiO_2 film on fuse quartz was synthesized at 600 °C without the pre-treatment process for 15 min with the N_2 flow rate of 1000 mL/min was investigated. The titania thin film reveals only anatase TiO_2 . The crystal structure of the TiO_2 film was anatase TiO_2 with 300-1000 nm thickness, depending on the reaction time. These results show achievement in preparing the titania thin films from our installed CVD rig. The influences of the Na^+ on titania phase formation were investigated by varying three different concentrations of NaOH solutions (including 0.25 M, 0.5 M, 1.0M and 2.0 M) in the pre-

treatment process. The terminologies of as-prepared titania thin films were 0.25M_Na, 0.50M_Na, 1.0M_Na and 2.0M_Na, respectively. The titania thin films were characterized by XRD, SEM, and SEM/EDX.

The titania thin film samples derived from the modified CVD method with Na⁺ pre-treatment substrates were characterized by Powder XRD, as shown in Figure 1(left). All models showed peak patterns corresponding to the main phases of anatase TiO₂ (JCPDS:04-014-8515) with a preferred growth direction in the [001] as seen by a very strong peak at $2\theta = 37.8^\circ$ of (004) lattice spacing, and minority phase of TiO₂(B) (JCPDS:04-007-6246) with an increasing proportion of TiO₂(B) in the titania film when using a higher concentration of NaOH at the substrate pre-treatment method. The XRD patterns show a preferred growth direction of TiO₂(B) of [110] lattice spacing as seen by an extreme peak at $2\theta = 24.9^\circ$ corresponding with the previous reports by Chimupala et al. The mechanism of deposition of TiO₂ thin films from TTIP thermal decomposition in CVD system is proposed by Fictorie et al.(Fictorie et al., 1994). The possible reaction is shown in equation (1). Thus, only TiO₂ can be deposited onto the substrate. The phase formation of TiO₂ depends on the reaction temperature (usually is the anatase phase when the temperature is lower than 700 °C whereas the temperature over 700 °C promotes the rutile TiO₂ structure)



A migration of Na⁺ through the deposited nascent titanium oxide during the deposition process is the main mechanism for producing TiO₂(B) (Chimupala et al., 2014a,b). In the same case, the TiO₂(B) phase was promoted with a very high percent composition in the thin film products due to the migration of Na⁺. This means that the more Na⁺ from NaOH solution provides, the more probability of Na⁺ migration encouraging the TiO₂(B) formation which was previous proposed by Chimupala, Y. et al. (Chimupala, Y. et al., 2014b, 2016). However, an XRD pattern of 2.0 M_Na shows low-intense peaks of an intermediate Na₂Ti₆O₁₃ phase due to the Na-rich zone. The crystallite sizes derived from the XRD line broadening in Figure 1(left) were estimated to be 49-60 nm for anatase TiO₂ and TiO₂(B), as presented in Table 1.

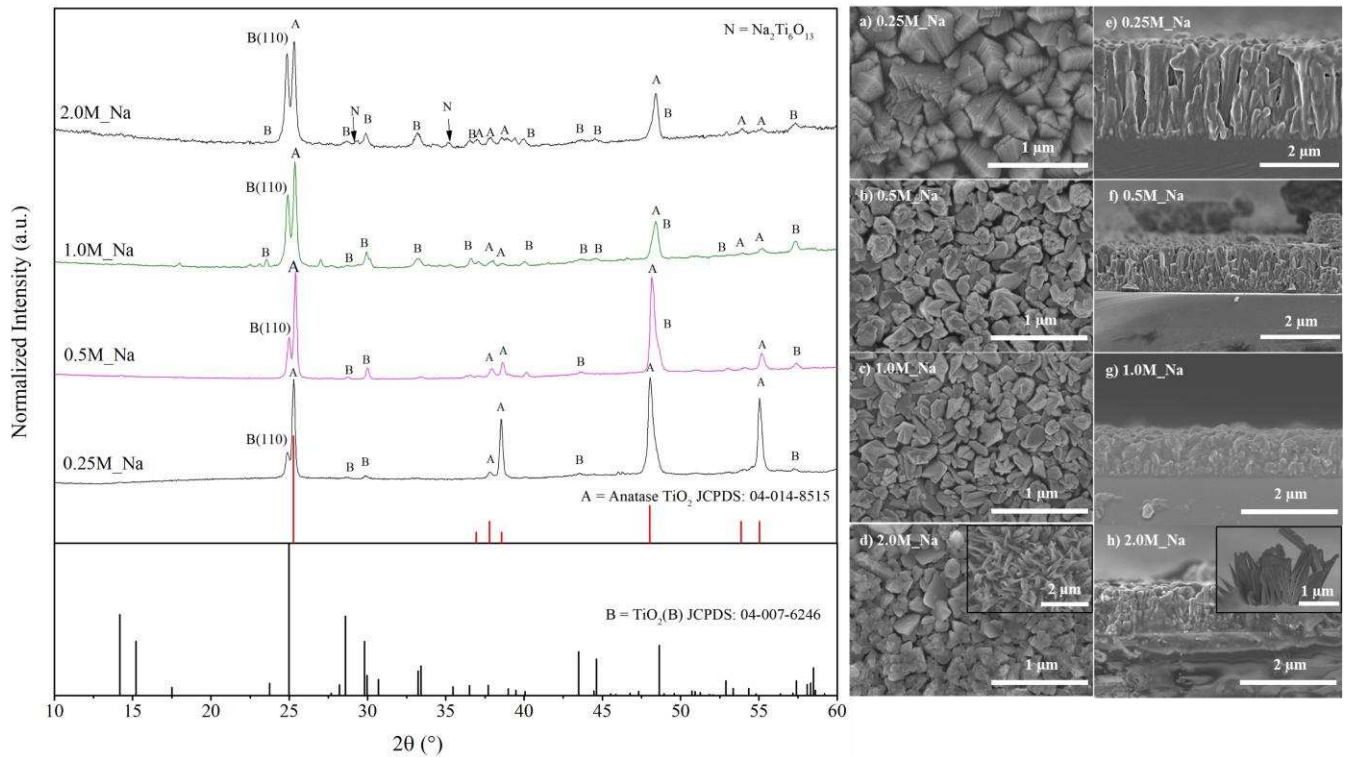


Figure 1 (left) XRD patterns of titania/titanate thin film samples deposited onto quartz substrates pre-treated by spraying NaOH solution in four concentrations of 0.25 M, 0.5 M, 1.0M and 2.0 M. and (right) SEM images of titania thin films prepared from modified CVD with NaOH pre-treatment at different concentrations: (a)-(d) are top-view surface morphologies from 0.25M_Na, 0.50M_Na, 1.0M_Na and 2.0M_Na respectively, and (e)-(h) are cross-section thin films from 0.25M_Na, 0.50M_Na, 1.0M_Na and 2.0M_Na respectively. Inset images in (d) and (h) are Na₂O needle particles that appear in 2.0M_Na sample.

Table 1 Calculated crystallite size from XRD patterns of the synthesized titania thin film samples by a modified CVD method with NaOH pre-treatment and results of SEM/EDX quantitative elemental analysis, measured aggregate particle size and film thickness derived from SEM images.

Sample	Calculated crystallite size from Scherrer's equation (nm)		Measured particle size (nm)	Measured film thickness (nm)	%Atomic		
	TiO ₂ (B)	Anatase			Na	Ti	O
0.25M_Na	61.5±5.0	49.9±5.0	368.4±2.0 (S.D. = 97.6)	2436.1±5.0 (S.D. = 97.6)	0.56	31.57	64.39
0.50M_Na	49.8±5.0	61.5±5.0	190.6±2.0 (S.D. = 61.7)	1174.8±5.0 (S.D. = 44.4)	1.46	30.73	65.19
1.0M_Na	49.8±5.0	48.9±5.0	145.6±2.0 (S.D.=57.2)	1092±5.0 (S.D. = 65.5)	2.10	32.74	65.16
2.0M_Na	49.8±5.0	49.8±5.0	131.6±2.0 (S.D. = 53.8)	959.2±5.0 (S.D. = 50.6)	2.52	33.38	53.65

Top-viewed SEM images of 0.25M_Na, 0.50M_Na, 1.0M_Na, and 2.0M_Na samples were also obtained to study the surface morphology and are represented in Fig. 1(right) (a) (b) (c) and (d) respectively. The concentrations of NaOH directly affect the particle morphology. At a low concentration of 0.25 M NaOH, the stack-like plate particle shape was presented. The polygonal particles and irregular shape morphologies were observed in 0.50 M_Na, 1.0 M_Na, and 2.0 M_Na, respectively. Interestingly, the 2.0 M_Na exhibited unique needle-like morphologies on the surface of TiO₂ thin films (just some area, less than 5%), shown in Fig. 1(right)(d) and Fig. 1(right)(h). The needle-like morphologies were finely characterized by the SEM-EDS technique to confirm the elemental compositions of the Na-rich zone, as shown in Fig. S1. It can be assumed from the EDS results that the needle morphology is Na₂O. The average particle sizes from the top surface derived from SEM plan-view images for 0.25M_Na, 0.50M_Na, 1.0M_Na, and 2.0M_Na samples are 368.4 ± 2.0 (S.D. = 97.6), 190.6 ± 2.0 (S.D. = 61.7), 145.6 ± 2.0 (S.D. = 57.2) and 131.6 ± 2.0 (S.D. = 53.8) respectively. The results were statistically manipulated by Image-J software and represented in Table 1.

The SEM cross-section of the samples showed a uniformed columnar structure with a film thickness of approximately 2436.1 ± 5.0 (S.D. = 119.8), 1174.8 ± 5.0 (S.D. = 44.4), 1092.6 ± 5.0 (S.D. = 65.5) and

959.2 ± 5.0 (S.D. = 50.6) nm for 0.25M_Na, 0.50M_Na, 1.0M_Na and 2.0M_Na samples, respectively. The cross-section morphology exhibited a columnar structure with different sizes of particles. Small columnar morphologies were deposited at interfaces between the substrates and TiO₂ layers, while the upper columnar particles were bigger in particle size. Also, the element compositions were investigated through SEM/EDX analysis, represented in Table 1, illustrating the presence of Na, Ti, and O in the samples, which match the XRD results.

3.2 The influences of Li⁺ ion on the formation of titania thin films

The influences of the Li⁺ on titania phase formation were investigated by varying four different concentrations of LiOH solutions (including 0.25 M, 0.50 M, 1.0 M, and 2.0 M) in the pre-treatment process. The synthesized titania thin films were labelled as 0.25M_Li, 0.50M_Li, 1.0M_Li, and 2.0M_Li, respectively. The titania thin films were then investigated by XRD, SEM, and SEM/EDX. The result showed that the XRD patterns of the as-prepared thin films were illustrated in Figure 2(right). XRD patterns showed peak patterns corresponding to the main phases of anatase TiO₂(JCPDS:04-014-8515), rutile TiO₂(JCPDS:04-007-5987), and Li₂TiO₃ (JCPDS:00-033-0831) with minority phase of brookite.

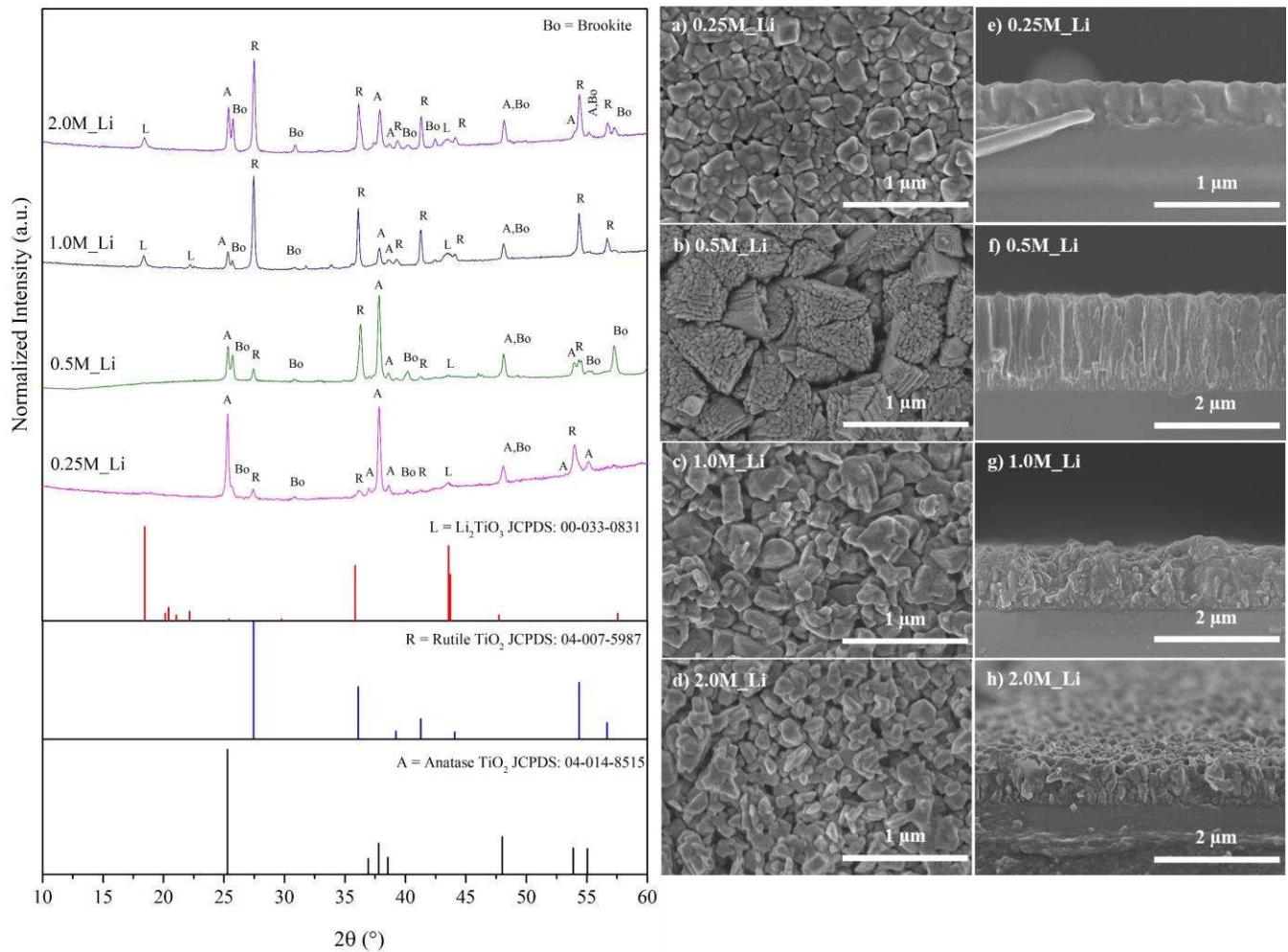


Figure 2 (left) XRD patterns of titania/titanate thin film samples deposited onto quartz substrates, pre-treated by spraying LiOH solution in four different concentrations of 0.25 M, 0.5 M, 1.0 M, and 2.0 M, and (right) SEM images of titania thin films prepared from modified CVD with LiOH pre-treatment at different concentrations: (a)-(d) are top-view surface morphologies from 0.25M_Li, 0.50M_Li, 1.0M_Li and 2.0M_Li respectively and (e)-(h) are cross-section thin films from 0.25M_Li, 0.50M_Li, 1.0M_Li and 2.0M_Li respectively.

The results revealed that while the anatase phase is a typical product from this normal CVD condition at 600 $^\circ\text{C}$, all the patterns derived from modified CVD samples indicated mixed titania and titanate phases, consisting of anatase, rutile, brookite, and lithium titanate (Li_2TiO_3) in varying proportions. The anatase pattern showed a preferred growth direction in the [001] as seen by a mighty peak at $2\theta = 37.8^\circ$ of (004) lattice spacing. Unexpectedly, no evidence for $\text{TiO}_2(\text{B})$ can be seen in any of the XRD patterns, even at high or low concentrations of Li^+ , indicating that $\text{TiO}_2(\text{B})$ cannot be synthesized by the substrate pre-

treatment with LiOH pre-treatment in the modified CVD method. When the concentration of LiOH was lower than 0.50 M, the majority phase was anatase. However, the majority phase of the films was changed to be rutile when the concentration of Li⁺ was increased to 1.0 and 2.0 M. Interestingly, the titania phases of brookite and rutile had not seen to be produced in this synthesis condition which is untypical at 600 °C for CVD preparation system. Therefore, it can be assumed that during the Li⁺ ions are migrating into nascent titania films and keep moving to the adjacent titania structure, it promotes the formation of the rutile structure after the Li⁺ ion leaves the host structure which was previous proposed by Svora et al. (2020).

The relative proportion of the brookite phase seems to be constant with the higher level of Li⁺ concentrations. Therefore, a higher Li⁺ concentration encouraged an increase in the relative proportion of rutile and Li₂TiO₃ in the thin films. The calculated crystallite sizes of anatase, rutile, and Li₂TiO₃ derived using Scherrer's equation were all about 40-50 nm, and the individual details of each sample are summarized in Table 2. The calculated crystallite size of brookite in each sample was not evaluated due to a small amount of brookite in the samples and the overlapping between the brookite peak and Anatase peak at $2\theta \approx 26^\circ$.

SEM micrographs were used to study the morphologies of the thin film samples. The SEM plan-view and SEM cross-sectional images of the thin film samples are shown in Fig. 2(right). Thin film samples with the same molar concentration of alkali metal ions were investigated. SEM plan-view images of 0.25M_Li, 0.5M_Li, 1.0M_Li, and 2.0M_Li are shown in Fig. 2 (right)(a), (b), (c), and (d), respectively. All showed dense films consisting of similar morphology of equiaxial grains. However, 0.5M_Li also illustrated agglomerated particles. The average particle sizes derived from SEM images of the particles from the top surface of the films in 0.25M_Li, 0.5M_Li, 1.0M_Li, and 2.0M_Li are 136 ± 2.0 (S.D. = 5.4), 521 ± 10.0 (S.D. = 148.1), 176 ± 2.0 (S.D. = 80.1), and 132 ± 2.0 (S.D. = 43.2), respectively.

Table 2 List of synthesized samples following LiOH pre-treatment with SEM/EDX quantitative elemental analysis results, measured aggregate particle size and film thickness derived from SEM images by Image-J software.

Sample	Measured particle size (nm)	Measured film thickness (nm)	%Atomic percent		
			Li	Ti	O
0.25M_Li	136 ± 2.0 (S.D.=5.4)	371.4 ± 5.0 (S.D.=14.8)	N/A	13.5	46.2
0.5M_Li	521 ± 10.0 (S.D.=148.1)	1628.0 ± 5.0 (S.D.=41.9)	N/A	32.2	62.5
1.0M_Li	176 ± 2.0 (S.D.=80.1)	996.1 ± 5.0 (S.D.=55.4)	N/A	19.2	64.5
2.0M_Li	132 ± 2.0 (S.D.= 43.2)	680.0 ± 5.0 (S.D.=47.2)	N/A	17.2	56.3

Furthermore, the individual SEM/EDX results relevant to the different LiOH concentrations in the pre-treatment process are given in Table 2. It can be clearly seen that the EDX results confirm the existence of titanium oxide. The relative atomic composition of Ti, O, and alkali metals may be affected by the electron beam interaction with the quartz substrate (in a very thin film case) or by an inhomogeneous region of spraying by LiOH. However, it cannot be detected retention of Li in the individual samples because of the limitation of the EDX technique for such light elements as Li. It can be concluded that the SEM/EDX results confirm the existence of Ti and O inside the sample and well corroborate with the XRD results, which contain anatase TiO₂, rutile TiO₂, brookite TiO₂, and lithium titanate (Li₂TiO₃) in varying proportions.

The film thicknesses and physical morphologies have been investigated in SEM cross-sectional images illustrated in Fig. 2 (right)(e), (f), (g), and (h) of 0.25M_Li, 0.5M_Li, 1.0M_Li, and 2.0M_Li samples, respectively. Generally, the film thickness remains constant when the synthesis conditions (CVD process) are nearly similar. However, these film thicknesses are variable, with approximate thicknesses of 371, 1628, 996, and 680 nm in 0.25M_Li, 0.5M_Li, 1.0M_Li, and 2.0M_Li samples, respectively. In addition, all SEM images show a columnar structure of the titania particles, obviously seen in the 0.5M_Li sample.

3.3 The influences of K^+ ion on the formation of titania thin films

The consequences of the synthesis parameters were investigated by varying the different concentrations of KOH solution in the pre-treatment process. The titania thin films were characterized by XRD, SEM, and SEM/EDX.

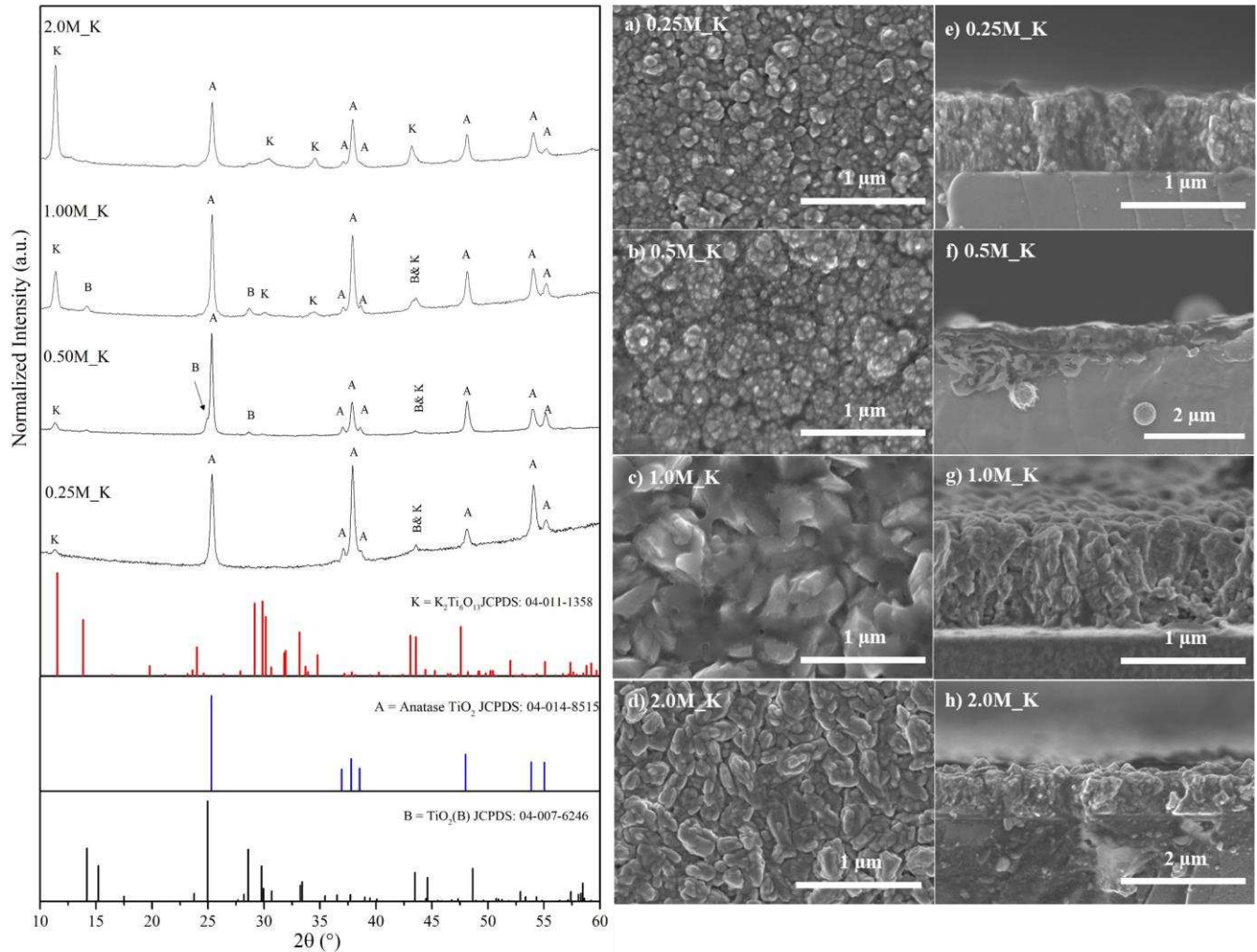


Figure 3 (left) XRD patterns of K^+ pre-treatment samples at different concentrations of 0.25 M, 0.50 M, 1.0 M, and 2.0 M of K^+ from KOH. And (right) SEM images of titania thin films prepared from modified CVD with KOH pre-treatment at different concentrations: (a)-(d) are top-view surface morphologies from 0.25 M_K, 0.50 M_K, 1.0 M_K and 2.0 M_K respectively and (e)-(h) are cross-section thin films from 0.25 M_K, 0.50 M_K, 1.0 M_K, and 2.0 M_K respectively.

Pre-treatment of fused quartz substrates by spraying with four different concentrations of KOH solutions (0.25 M, 0.50 M, 1.0 M, and 2.0 M) was studied. The nomenclatures of the final products were 0.25 M_K, 0.50 M_K, 1.0 M_K, and 2.0 M_K, respectively. The XRD patterns of the films are shown in Fig. 3(left). There had no evidence from four samples that exhibited obvious peaks due to $\text{TiO}_2(\text{B})$. However, the optimum conditions to promote $\text{TiO}_2(\text{B})$ phase formation appear to lie between the 0.50 M_K and 1.0M_K samples corresponding with KOH concentration in the range of 0.50 M to 1.0 M NaOH. Therefore, it is unsurprising that anatase TiO_2 appeared for every sample and was the main component of the titania films. Moreover, a monoclinic phase of $\text{K}_2\text{Ti}_6\text{O}_{13}$ unpredictably appears in every sample; it became the major component in the titania thin films when the concentration of KOH is higher than 2.0 M. The crystallite sizes for anatase TiO_2 and $\text{K}_2\text{Ti}_6\text{O}_{13}$, calculated from XRD line broadening and Scherrer's equation, were all estimated to be in the range of 12-80 nm (*see* Table 3).

Different concentrations of KOH solution in the pre-treatment process significantly promote other phase formations. At low KOH concentration, it seems to encourage the formation of anatase TiO_2 , whereas, at high KOH concentration, $\text{K}_2\text{Ti}_6\text{O}_{13}$ is the majority in the titania thin films (Svora et al., 2020). The thin film samples also presented the coexistence of the $\text{TiO}_2(\text{B})$ phase and anatase. However, it appeared that K^+ ions had a limitation in promoting the $\text{TiO}_2(\text{B})$ phase and preferred to form $\text{K}_2\text{Ti}_6\text{O}_{13}$ instead, as seen from the relative intensity of the peaks in XRD results.

Table 3 Calculated crystallite size from XRD patterns of the synthesized titania thin film samples by a modified CVD method with KOH pre-treatment and results of SEM/EDX quantitative elemental analysis, measured aggregate particle size and film thickness derived from SEM images.

Sample	Calculated crystallized size (nm)		Measured particle size (nm)	Measured film thickness (nm)	Atomic percent composition from SEM/EDX		
	Anatase	K ₂ Ti ₆ O ₁₃			K	Ti	O
0.25M_K	38 ± 5.0	18 ± 5.0	79 ± 2.0 (S.D.=27)	637±5.0 (S.D.=29)	0.2	15.2	48.7
0.50M_K	51 ± 5.0	36 ± 5.0	67 ± 2.0 (S.D.=31)	752±5.0 (S.D.=133)	0.4	20.7	54.3
1.0M_K	43 ± 5.0	26 ± 5.0	229 ± 2.0 (S.D.=68)	846±5.0 (S.D.=25)	1.4	17.6	69.6
2.0M_K	43 ± 5.0	32 ± 5.0	150 ± 2.0 (S.D.=110)	764±5.0 (S.D.=77)	1.7	17.8	62.0

SEM images examined the morphology of synthesized titania thin films. The SEM plan-view images and SEM cross-sectional of the KOH pre-treatment samples were presented in Figure 3(right). The difference in grain shapes was observed with increasing KOH concentration. All show dense thin films consisting of irregular-shaped grains for 0.25 M_K, 0.50 M_K, 1.0 M_K, and polygonal-shaped grains for 2.0 M_K. The average aggregated particle sizes derived from SEM images of the particles from the top surface of the films in 0.25 M_K, 0.50 M_K, 1.0 M_K, and 2.0 M_K are 79, 67, 229, and 150 nm, respectively. The film thicknesses and physical morphologies have been investigated in SEM cross-sectional images illustrated in Fig. 3(right) (e)-(h) of 0.25 M_K, 0.50 M_K, 1.0 M_K, and 2.0 M_K samples. The film thicknesses were in the range of 300-700 nm with approximate thicknesses of 637, 752, 846, and 764 nm in 0.25 M_K, 0.50 M_K, 1.0 M_K, and 2.0 M_K samples, respectively. The average aggregated particle sizes and film thicknesses are summarized in Table 3. SEM/EDX determined the elemental analysis of all thin film samples. The results relevant to the different KOH concentrations in the pre-treatment process were given in the same table (Table 3). It can be clearly seen that the EDX results confirm the existence of titanium oxide with retention of K in the individual samples corresponding to the KOH solution used in the pre-treatment process. The atomic percentages of K increase with an

increase in KOH concentration. This means that the alkali metal ions in the titania/titanate thin films depend directly on the concentration of the alkali metal solution applied. These results correlated with the XRD patterns.

3.4 Titania/Titanates formation mechanism

The proposed mechanism of $\text{TiO}_2(\text{B})$ phase formation resulting from alkaline ions substrate pre-treatment was regarded as alkaline titanate transformation through a modified CVD process. In the case of the substrate pre-treatment with NaOH solution, the hydroxide layers were deposited onto the fused quartz substrate. Then, these layers were decomposed to form Na_2O during a 600 °C pre-heated temperature following this chemical reaction $2\text{NaOH} \rightarrow \text{Na}_2\text{O} + \text{H}_2\text{O}$ (Yurkinskii et al., 2005). Therefore, we believed the formation mechanism might first develop the intermediated titanate phase and then transform it into $\text{TiO}_2(\text{B})$ (Etacheri et al., 2013; Liu et al., 2014). In this case, the intermediate phase should be $\text{Na}_x\text{Ti}_y\text{O}_z$ compound before creating $\text{Na}_2\text{Ti}_6\text{O}_{13}$, then convert to $\text{TiO}_2(\text{B})$.

During the CVD process, Na^+ ions could migrate from the low-concentrated area of Na to the higher-concentrated site. The thermal energy arising from the heating process might increase the possibility of diffusion of Na^+ ions, breaking Na–O bonding and leaving Na^+ ions to be more mobile likely. The Na^+ ions may diffuse into the deposited TiO_2 layer from the TTIP decomposition. This process could cause the intermediated sodium titanate phase, e.g., $\text{Na}_2\text{Ti}_6\text{O}_{13}$ depending on the ratio of the binary phase system of Na_2O – TiO_2 phase diagram (Eriksson and Pelton, 1993). According to the SEM/EDX results, Na/Ti contained inside the 2.0M_Na sample was the highest ratio. This might promote the formation of $\text{Na}_2\text{Ti}_6\text{O}_{13}$, which appeared in the XRD pattern of the 2.0M_Na sample. There was some evidence showing that $\text{Na}_2\text{Ti}_6\text{O}_{13}$ with a stepped-like crystal structure was likely promoted as the intermediate phase from the modified CVD synthesis, as shown in the following reaction $\text{Na}_2\text{O} + 6\text{TiO}_2 \rightarrow \text{Na}_2\text{Ti}_6\text{O}_{13}$. The reaction exhibited a spontaneous process due to the negative Gibbs free energy of the reactions ($\Delta G = -2416.13$ kJ/mol), calculated in accordance with NIST-JANAF thermodynamical tables (Eriksson and Pelton, 1993; Malcolm W. Chase, 1990). This means the reaction of $\text{Na}_2\text{O} + 6\text{TiO}_2 \rightarrow \text{Na}_2\text{Ti}_6\text{O}_{13}$ is more

straightforward and likely to occur when compared to other alkaline titanates' chemical reactions requiring less energy before proceeding.

The intermediate phase may act as the template for promoting $\text{TiO}_2(\text{B})$. However, Na^+ ions in the interlayer structure of $\text{Na}_2\text{Ti}_6\text{O}_{13}$ could diffuse out of the crystal framework due to the absorbed thermal energy. This causes an unstable structure if the system leaves a void template between TiO_6 octahedral structures. Furthermore, considering the interlayer spacing, if the stepped layers of $\text{Na}_2\text{Ti}_6\text{O}_{13}$ (~0.32 nm) are close to the pore size (~0.32 × 0.25 nm) of the structure of $\text{TiO}_2(\text{B})$ in a similar direction, the TiO_6 octahedral building block could therefore rearrange or shrink to form $\text{TiO}_2(\text{B})$.

For the K^+ ion pre-treatment sample, the proposed mechanism was slightly different due to the crystal structure of the final product. The formation of potassium titanate and $\text{TiO}_2(\text{B})$ was described as follows. KOH layers on the substrate were heated and then transformed into K_2O and H_2O molecules. The K^+ ions can diffuse like those of the Na^+ ions. According to the K_2O - TiO_2 binary system (Eriksson and Pelton, 1993), the system exhibited only TiO_2 and $\text{K}_2\text{Ti}_6\text{O}_{13}$ phases when considering the fraction of $\text{TiO}_2/\text{K}_2\text{O}$ is approximately 1.0 at 600 °C. The phase diagram agreed with the XRD patterns of the potassium pre-treatment samples, which illustrated mixed phases of the $\text{TiO}_2(\text{B})$ and $\text{K}_2\text{Ti}_6\text{O}_{13}$. According to Svora et al., TiO_2 prepared samples annealed at 800°C showed the presence of $\text{K}_2\text{Ti}_6\text{O}_{13}$ and an unknown phase at $2\theta=15^\circ$ and 43° , which are characteristic XRD peaks of $\text{TiO}_2(\text{B})$ (Svora et al., 2020). The potential chemical reaction followed the equation, $\text{K}_2\text{O} + 6\text{TiO}_2 \rightarrow \text{K}_2\text{Ti}_6\text{O}_{13}$, where the total Gibbs free energy of this reaction was about -2256.41 kJ/mol (Eriksson and Pelton, 1993; Malcolm and Chase, 1990). This value illustrated the difficulty in initiating the reaction compared to those of Na^+ ion pre-treatment samples.

Similar to those of $\text{Na}_2\text{Ti}_6\text{O}_{13}$, the intermediate phase of $\text{K}_2\text{Ti}_6\text{O}_{13}$ (Monoclinic structure) with a stepped-like layer of TiO_6 octahedra could be transformed, allowing the diffusion of the K^+ ions between the interspacing layers of the titanate structure. This left vacancies inside the structure, enabling structural reform to promote $\text{TiO}_2(\text{B})$ phase formation. The ionic radius ratio per interlayer spacing of $\text{K}_2\text{Ti}_6\text{O}_{13}$ (~36.13%) is significantly higher than that of $\text{Na}_2\text{Ti}_6\text{O}_{13}$ (~31.87%). This implied that the higher ratio

represented the problematic mobility of the K^+ ions into the interspace layers. Additionally, K^+ ions have a higher mass than Na^+ , resulting in a slower diffusion rate of the ions in the medium. This could leave K^+ ions in the final structure of the titanate during the transformation process and cause the production of $K_2Ti_6O_{13}$ rather than $TiO_2(B)$. When the concentration of the K^+ was increased, more potassium titanate was found, which means that they would remain in the crystal structure forming $K_2Ti_6O_{13}$ as appeared in the XRD profile (*see* Fig. 3(left)).

The diffusion of alkali metal ions into the crystal structure of alkaline titanate was also computationally conducted to support these hypotheses. In Fig. 4(a), the results demonstrated that, for potassium and sodium hexa-titanate, the alkali metal (A) atoms are stable in the site surrounded by six neighboring oxygen atoms (Kataoka et al., 2011). After removing an A atom, the two A atoms next to the vacancy site in the *b*-direction slightly shift to the defect site. Furthermore, we used the CINEB method to find the minimum energy path for A atom diffusion from an initial configuration (IS) where A atom next to the vacancy site starts to replace the vacancy at the final configuration (FS) shown in Figure 4(a). We found that the transition state (TS) of the diffusion occurred while the A atom was passing through the tunnel between terminal oxygens. These alkaline ions could continuously migrate to new layers of TiO_2 thin films resulting in more $TiO_2(B)$ phase formation in the system. In the absence of Na^+ ions in the structure, the anatase phase can be formed. Additionally, the synthesized $TiO_2(B)$ with exceeded energy from thermal energy during the heating process can transform into anatase structures due to its meta-stable $TiO_2(B)$ phase (Banfield et al., 1991; Brohan et al., 1982).

In Fig. 4(b), the energy barriers, which respect the different energy between TS and IS, are calculated to be 1.65 and 0.50 eV in the case of K^+ and Na^+ , respectively. The calculated energy barrier in the case of Na^+ agree well with the experimental value of 0.56 eV (Fukuzumi et al., 2016). It should be noted that the barrier of K^+ diffusion is significantly larger than that of Na because of the larger ionic radius leading to the strong interaction with terminal oxygens in the TS state. These energy barrier calculations were in good agreement with those of Gibbs's free energy calculation. Therefore, it can be implied that the

substrate pre-treatment with K^+ ions was challenging to promote $TiO_2(B)$ due to its system structure and ionic size.

Interestingly, the $TiO_2(B)$ phase cannot be promoted in the case of Li^+ ions pre-treatment. Therefore, only mixed phases of titanate, including anatase, rutile, brookite, and Li_2TiO_3 thin films, were fabricated. When the concentration was increased, the majority phase was changed from anatase to rutile, indicating that the more Li^+ ion in the system resulted in the more stable stage of titanate thin films. During the modified CVD, the reaction was driven into the binary system of Li_2O-TiO_2 (Izquierdo and West, 1980). The intermediate phase of $Li_xTi_yO_z$ could depend on the composition of each element.

For computational prediction of lithium hexa-titanate, the crystal structure of lithium titanate exhibited parallel layered structures with Li^+ ions located between the layers. Interestingly, there was no close structure like sodium and potassium titanate. It is noted that Li atoms are more stable in a tunnel surrounded by three terminal oxygens instead of the 6-oxygen-coordinated site like K and Na atoms. This is due to the smaller ionic radius of the Li atom. This finding is consistent with previous experiment (Kataoka et al., 2011). For the diffusion, we find that the migrated Li is not moved directly like in other cases, but it moves upward in an *a*-direction to bond with two oxygen atoms in the TS state as shown in Fig. 4(a). Note that the interaction of Li and O in the TS state is not so strong that the shape of the energy profile in the case of Li diffusion gets a flatter band in near the TS configuration, as shown in Fig. 4(b). The diffusion pathway and TS configuration were in good agreement with that reported in previous study (Kuganathan et al., 2019). The corresponding energy barrier is only 0.28 eV, which is consistent with that obtained in other previous DFT calculation (0.25 eV) (Kuganathan et al., 2019) and experimental value (0.28 eV) (Fukuzumi et al., 2016).

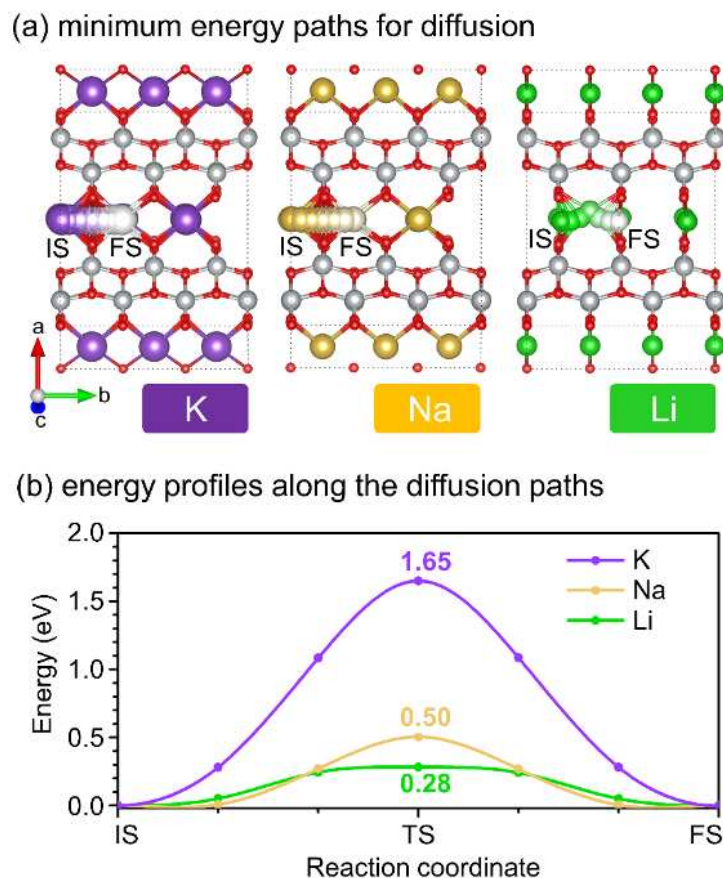


Figure 4 (a) Illustration of crystal structures and the minimum energy paths for alkaline (A) vacancy diffusion in alkaline hexa-titanate ($A_2Ti_6O_{13}$) from an initial configuration (IS) to final configuration (FS), where $A = K, Na,$ and Li . (b) the corresponding energy profiles along the diffusion paths and the associated energy barriers. The atoms are colored as purple, orange, green, gray, and red, representing K, Na, Li, Ti, and O, respectively.

In this case, Li_2TiO_3 was promoted, as shown in the XRD pattern (*see* Fig. 2(left)). The potential chemical reaction was $Li_2O + TiO_2 \rightarrow Li_2TiO_3$, a spontaneous reaction with negative values ($\Delta G = -261.62$ kJ/mol).³⁵ This supports that Li^+ ions are the most difficult to promote $TiO_2(B)$ according to their diffusion profile. Our findings were excellent and agreed with the previous study of Li^+ and Na^+ intercalation in titanate structure, and the diffusion coefficients were $D_{Li^+} \sim 10^{-11}$ cm^2/s and $D_{Na^+} \sim 10^{-16}$ cm^2/s . (Yu et al., 2013) This could imply that Li is the lighter element than Na and K; thus, it tends to move fastest. Additionally, the ionic radius and interspacing layers ratio was the lowest value ($\sim 29.01\%$) among these three titanates. When Li^+ ions diffuse out from the interlayer spacing, the crystal structure may rapidly shrink, resulting in a more close-pack titanate structure (such as brookite and rutile).

3.5 Photocatalysis for Dye Degradation

A 15 mL of 5×10^{-6} M (1.59 mg/L) methylene blue solution was selected as a model dye pollutant in wastewater. As shown in Figure 5, the degradation efficiencies of each 10 mm \times 10 mm thin film sample were presented by column chart for studying the effect of using K^+ , Na^+ and Li^+ involved titania/titanate catalysts and the concentration of alkali source. All samples presented the photocatalytic active thin films relative to a catalyst-free result (w/o sample). In the context of environmental impact of using alkali metal cations to promote the mixed phase formation of TiO_2 for the better photocatalytic activity, the alkali cation has less impact on environmental problem as they are high natural abundance in the earth crust, and natural water. Moreover, the alkali metal cations are trapped tightly in the titania structure and unable to release to the environment during the photodegradation process.

Of all the TiO_2 polymorphs, anatase is considered to be the most efficient photocatalyst. However, it has been shown that combining various phases of TiO_2 , such as anatase/rutile or anatase/ $TiO_2(B)$, results in a higher degree of photocatalytic effectiveness than pure anatase (Chimupala et al., 2016; Mohamed et al., 2012; Cross et al., 2012). The charge transfer mechanism between the various phases was directly impacted by the mixed phases, which may have reduced photo-generated electron recombination and increased photocatalytic activity (Li et al., 2008).

The highest methylene blue degradation was about 59.1% (*see* Fig. S2), derived from the 0.25M_Na sample. The relative ratio of anatase TiO_2 and $TiO_2(B)$ phases of 4:1 in the 0.25M_Na sample played an essential role in promoting higher photocatalytic activity, which is beneficial for improving efficiency by reducing recombination of photo-generated electrons and holes by using heterojunction anatase/ $TiO_2(B)$ (Chairungsri et al., Chimupala et al., 2016). However, 2.0 M_Na, 1.0 M_Na and 0.5 M_Na samples, containing an excess proportion of the $TiO_2(B)$ in the thin film samples, show a bit lower photocatalytic efficiency (50.6%, 46.0% and 48.4%, respectively) because the anatase phase typically has a higher photocatalytic activity than $TiO_2(B)$. However, mixing anatase/ $TiO_2(B)$ in the small $TiO_2(B)$ content has resulted in higher photocatalytic efficiency than solely pure anatase due to the heterojunction effect. In

contrast, the dominant $\text{TiO}_2(\text{B})$ on the mixed TiO_2 phases gave the worse photocatalytic efficiency because the nature of $\text{TiO}_2(\text{B})$ has low photocatalytic activity (Chairungsri et al., 2022).

As shown in Fig. 5, all the Na^+ pre-treated samples showed higher photocatalytic activities than the Li^+ and K^+ pre-treated samples. The mixed phases between dominant anatase TiO_2 and minor $\text{K}_2\text{Ti}_6\text{O}_{13}$ in the 0.50 M_K and 1.00 M_K samples encouraged the greater ability of the photocatalyst (34.2 and 32.2% respectively) than the nearly pure anatase phase as present in the 0.25 M_K sample (30.1%). Whereas the excess of $\text{K}_2\text{Ti}_6\text{O}_{13}$ in the mixed phases thin film sample (2.0 M_K) illustrated the lowest photocatalytic activity (21.8%) since the $\text{K}_2\text{Ti}_6\text{O}_{13}$ has very low photocatalytic activity.

Compared with Li^+ pre-treated samples, the ratio of ionic radius of Li^+ ion was found to be the lowest value among K^+ and Na^+ ions. When Li^+ ions diffuse out from the interlayer spacing of the titanate structure, the crystal structure may rapidly shrink, resulting in a more close-pack structure of titanates such as brookite and rutile. On the other hand, the Li^+ ion-free area in the titanate structure generally promotes the formation of anatase TiO_2 via the CVD process at 600°C . Therefore, the dominant anatase TiO_2 in the mixed three phases of the titania thin film samples occurred in the small amount of Li^+ ion pre-treated samples, such as 0.25 M_Li and 0.5 M_Li, showed a higher photocatalytic performance (49.6% and 45.5% respectively) than the Li^+ high content samples (39.8% in 1.0M_Li and 42.9% in 2.0M_Li). On the other hand, the rutile TiO_2 and brookite TiO_2 in 1.0M_Li and 2.0M_Li has very lower photocatalytic efficiency than anatase TiO_2 . Therefore, the preminent of rutile and brookite might promote defects in mixed phases heterojunction and provide a lower photocatalytic efficiency.

The photocatalytic-degradation efficiency of the fabricated titania/titanate thin films were compared with the previous reports in which TiO_2 thin films were used for organic dye removal applications, as shown in Table S2. The efficiency of our materials seems to be a bit lower than other works due to the smaller amount of catalyst coated on the substrates. However, this work emphasizes the beneficial usage of mixed-phase synthesis for greater degrading effectiveness, which can be considered a valuable alternative coating strategy.

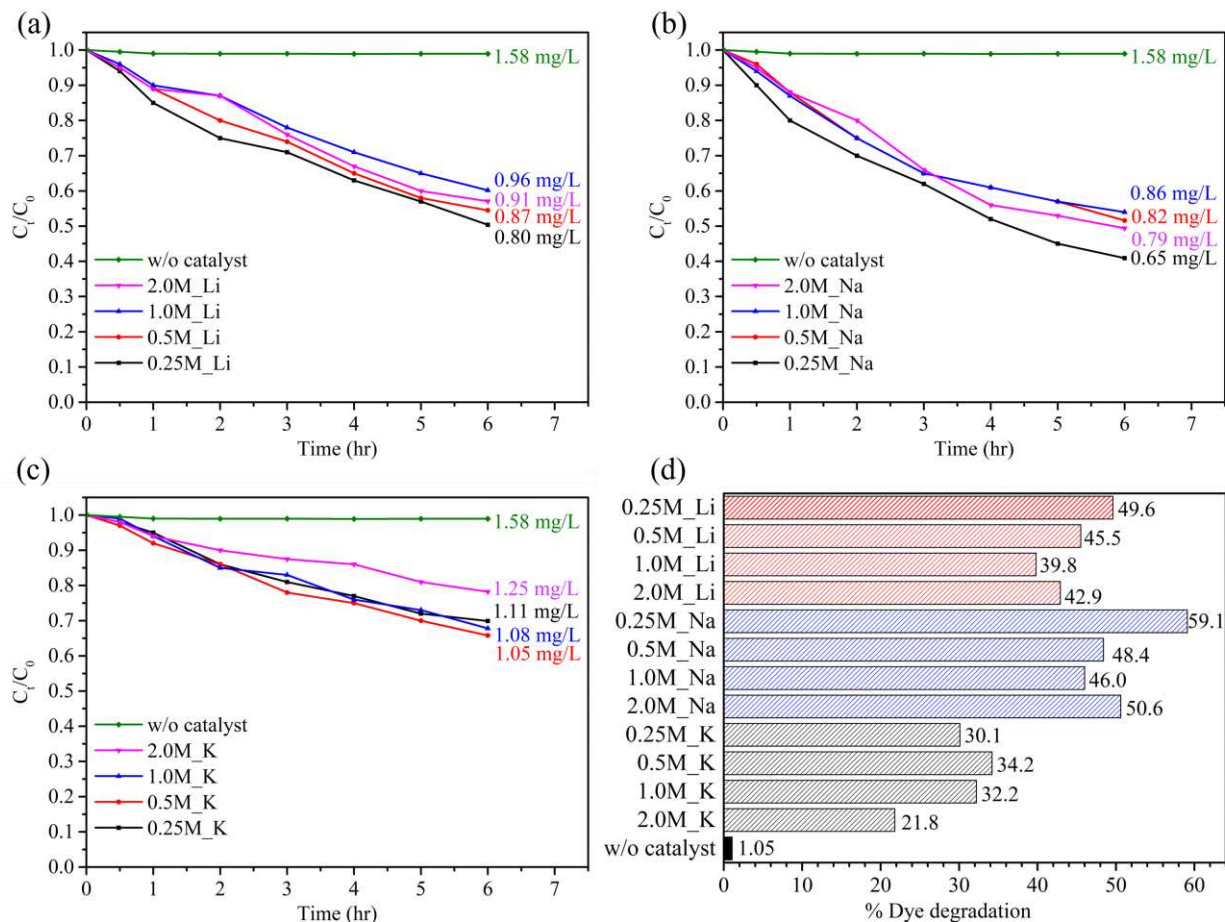


Fig. 5 The photocatalytic degradation efficiency for Methylene blue by titania/titanate phases thin film on fused quartz substrates synthesized by modified CVD with alkali metal pre-treatment by spraying (a) LiOH solution, (b) NaOH solution, (c) KOH solution in varied concentrations and (d) the summarized dye degradation performance.

To our knowledge, the first time a mixed titania/TiO₂(B) thin film was made using CVD with a modified substrate pre-treatment utilizing various alkali metal ion solutions. This proved how efficient the universal alkaline ions pre-treatment method was as a breakthrough synthesis technique for promoting pure/mixed TiO₂ thin films on any substrate with the potential for promising environmentally friendly applications particularly wastewater treatment. Even the photocatalytic degradation efficiency of mixed titania/TiO₂(B) thin film was very low compared with the TiO₂ nanoparticles and other immobilized TiO₂ samples (*see* Table S2). However, in the context of scalability, the CVD process is easy, and cost-effective to scale-up and reproduce especially in the soda lime glass manufacturing process. For example, TTIP vapor can be introduced into the coating chamber under ambient pressure after the molten glass passing

through the floating bath at surface temperature of c.a. 600 – 700 °C. The alkali metal cations in the soda lime glass precursors such as Na⁺ diffuse into the nascent titania layer during the TiO₂ thin film deposition forming mixed phase titania polymorphs on the glass. The economical evaluation for the photocatalysis using mixed phase TiO₂/titania thin film was investigated. The production cost of a 10 g catalyst (top surface c.a. 100 cm²) prepared by CVD of 5 mL TTIP solution on quartz or soda lime glass substrate was approximately 0.5 USD (Sigma Aldrich, 30 June 2023). For these reasons, this technology for producing mixed phase TiO₂/titania thin film on the fixed substrate is worth conducting on many industrial scales.

Moreover, the CVD technique can design the coating chamber as a continuous production line that makes this technique easy to scale up and have potential use in industrial scale, whereas the other deposition processes such as plasma deposition, atomic layer deposition require an extreme synthesis condition like vacuum chamber. In another way, hydrothermal, solgel, coprecipitation, have limitations to preparing the immobilized titania thin film on fixed substrate.

3.6 Practical Applications and Future Research Prospects

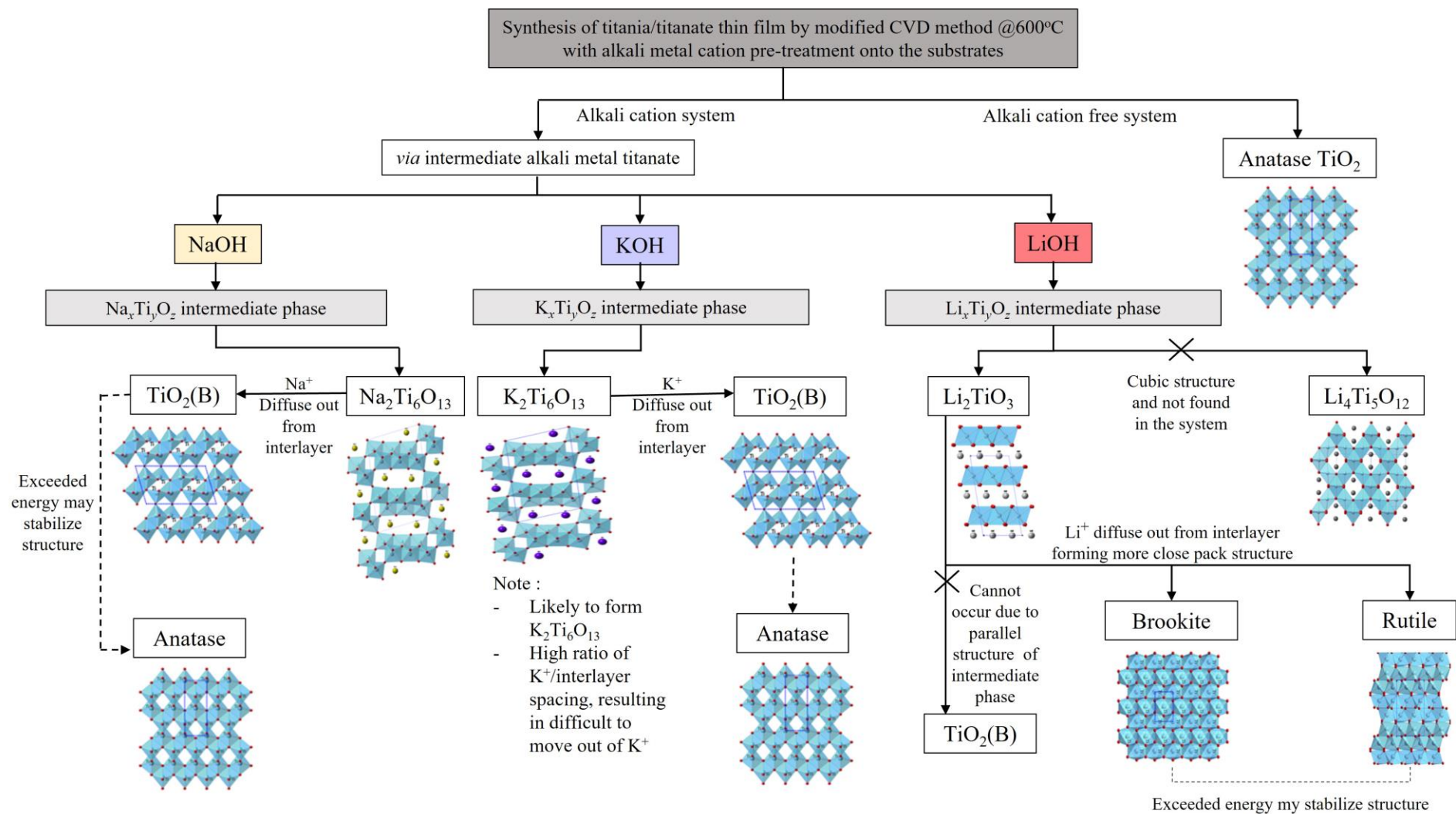
From this work, the immobilized mixed phase TiO₂/titania thin film on glass substrate was proven as a promising photocatalyst for methylene blue dye degradation. This was considered as a demonstration of a hazardous organic small molecule in polluted water. Therefore, the prepared materials can be applied in the catalytic reactor in both fixed bed and continuous wastewater treatment process. This immobilized photocatalytic thin film materials also show the advantages on the practical uses over than the mobilized one such as scalability, ease of use and reuse, and the absence of catalytic waste discharge during the catalytic cycle. In terms of future research direction of this work, not only the alkali metal cation but also the light alkaline-earth metal cations such as Mg²⁺, Ca²⁺ should be studied as an alternative pretreating reagent because of their abundance and chemical similarity. The diffusion of the alkaline-earth metal cations into the TiO₂/titania thin film might give interesting outcomes on the phase formation. Moreover, real water pollutants with hazardous organic molecules such as paraquat could be studied in the photocatalytic manner.

4. CONCLUSIONS

Nano-particulate titania/titanate thin films were deposited onto fused quartz substrates via the modified CVD method. TTIP and N₂ gas were used as a titanium precursor and a carrier gas, respectively, operating at 600 °C for 15 min. Without the alkali-metal hydroxide pre-treatment process, only the anatase TiO₂ was produced in the thin film samples. The titania/titanate phases of thin-film products synthesized by modified CVD with alkali metal pre-treatment of fused quartz substrates by spraying three different alkaline hydroxide solutions in varied concentrations were summarized in Table 4 and Fig. 6. The synthesized thin film was tested for photocatalytic activities. The highest methylene blue degradation was about 59.1%, derived from the 0.25 M_Na samples. The relative ratio of anatase and TiO₂(B) phases (4:1) in the 0.25 M_Na sample was one of the key factors to promote photocatalytic activity. All the Na⁺ pre-treated samples showed higher photocatalytic activities than the Li⁺ and K⁺ samples.

Table 4 Titania/titanate phase formation in the as-prepared thin films and photocatalytic activity

Alkali metal cation	Sample name	Phase composition in thin film samples *major, #minor, †insignificant	% Dye degradation
Li ⁺	0.25M_Li	Anatase*, Rutile [†] , Brookite [†] , Li ₂ TiO ₃ [†]	49.6
	0.50M_Li	Anatase*, Rutile [#] , Brookite [#] , Li ₂ TiO ₃ [†]	45.5
	1.00M_Li	Anatase [#] , Rutile*, Brookite [#] , Li ₂ TiO ₃ [†]	39.8
	2.00M_Li	Anatase [#] , Rutile*, Brookite [#] , Li ₂ TiO ₃ [#]	42.9
Na ⁺	0.25M_Na	Anatase*, TiO ₂ (B) [#]	59.1
	0.50M_Na	Anatase*, TiO ₂ (B) [#]	48.4
	1.00M_Na	Anatase*, TiO ₂ (B) [#]	46.0
	2.00M_Na	Anatase*, TiO ₂ (B)*, Na ₂ Ti ₆ O ₁₃ [†]	50.6
K ⁺	0.25M_K	Anatase*, K ₂ Ti ₆ O ₁₃ [†]	30.1
	0.50M_K	Anatase*, TiO ₂ (B) [†] , K ₂ Ti ₆ O ₁₃ [†]	34.2
	1.00M_K	Anatase*, TiO ₂ (B) [†] , K ₂ Ti ₆ O ₁₃ [#]	32.2
	2.00M_K	Anatase [#] , TiO ₂ (B) [†] , K ₂ Ti ₆ O ₁₃ [*]	21.8



1

2 **Fig. 6.** Schematic diagram summarizing the titania/titanate phase formation in the thin film samples synthesized by the modified CVD method using
 3 alkali metal cation pre-treatment of the fused quartz substrate.

4

ACKNOWLEDGEMENTS

This research work was financially supported through the Development and Promotion of Science and Technology Talent Projects (DPST) through the research funding for DPST graduates with first placement (Grant No. 011/2559). The Centre of Excellence in Materials Science and Technology, Chiang Mai University, Thailand and Research and Graduate Studies, Khon Kaen University, also partially supported this work. The authors would like to acknowledge Dr. Apinpus Rujiwatra from the Department of Chemistry, Faculty of Science, Chiang Mai University, for supervising the DPST research fund. In addition, NC would like to thank the young researcher development project of Khon Kaen University for his financial support.

Appendix A. Supplementary data

Supplementary data to this article can be found online at <https://doi.org/10.1016/j.envres.2023.117347>.

REFERENCES

- Bai, Y., Li, W., Liu, C., Yang, Z., Feng, X., Lu, X., Chan, K.Y., 2009. Stability of Pt nanoparticles and enhanced photocatalytic performance in mesoporous Pt-(anatase/TiO₂(B)) nanoarchitecture. *J. Mater. Chem.* 19, 7055–7061. <https://doi.org/10.1039/b910240j>
- Bai, Y., Mora-Seró, I., De Angelis, F., Bisquert, J., Wang, P., 2014. Titanium dioxide nanomaterials for photovoltaic applications. *Chem. Rev.* 114, 10095–10130. <https://doi.org/10.1021/cr400606n>
- Banfield, J.F., Veblen, D.R., Smith, D.J., 1991. The identification of naturally occurring TiO₂(B) by structure determination using high-resolution electron microscopy, image simulation, and distance-least-squares refinement. *Am. Mineral.* 76, 343–353.
- Blöchl, P.E., 1994. Projector augmented-wave method. *Phys. Rev. B* 50, 17953–17979. <https://doi.org/10.1103/PhysRevB.50.17953>
- Brohan, L., Verbaere, A., Tournoux, M., 1982. La transformation TiO₂(B) to anatase. *Mater. Res. Bull.* 17, 355–361.
- Carmichael, P., Hazafy, D., Bhachu, D.S., Mills, A., Darr, J.A., Parkin, I.P., 2013. Atmospheric pressure chemical vapour deposition of boron doped titanium dioxide for photocatalytic water reduction and oxidation. *Phys. Chem. Chem. Phys.* 15, 16788–16794. <https://doi.org/10.1039/c3cp52665h>

- Chairungsri, W., Subkomkaew, A., Kijjanapanich, P., Chimupala, Y., 2022. Direct dye wastewater photocatalysis using immobilized titanium dioxide on fixed substrate. *Chemosphere* 286, 131762. <https://doi.org/10.1016/j.chemosphere.2021.131762>
- Chen, X., Selloni, A., 2014. Introduction: Titanium Dioxide (TiO₂) Nanomaterials. *Chem. Rev.* 114, 9281–9282. <https://doi.org/10.1021/cr500422r>
- Chimupala, Y., Drummond-Brydson, R., 2018. Hydrothermal synthesis and phase formation mechanism of TiO₂(B) nanorods via alkali metal titanate phase transformation. *Solid State Phenom.* 283, 23–36. <https://doi.org/10.4028/www.scientific.net/SSP.283.23>
- Chimupala, Y., Hyett, G., Simpson, R., Brydson, R., 2014. Synthesis and characterization of a mixed phase of anatase TiO₂ and TiO₂(B) by low pressure chemical vapour deposition (LPCVD) for high photocatalytic activity. *J. Phys. Conf. Ser.* 522. <https://doi.org/10.1088/1742-6596/522/1/012074>
- Chimupala, Yothin, Hyett, G., Simpson, R., Mitchell, R., Douthwaite, R., Milne, S.J., Brydson, R.D., 2014. Synthesis and characterization of mixed phase anatase TiO₂ and sodium-doped TiO₂(B) thin films by low pressure chemical vapour deposition (LPCVD). *RSC Adv.* 4, 48507–48517. <https://doi.org/10.1039/c4ra07570f>
- Chimupala, Y., Junploy, P., Hardcastle, T., Westwood, A., Scott, A., Johnson, B., Brydson, R., 2016. Universal synthesis method for mixed phase TiO₂(B)/anatase TiO₂ thin films on substrates via a modified low pressure chemical vapour deposition (LPCVD) route. *J. Mater. Chem. A* 4, 5685–5699. <https://doi.org/10.1039/C6TA01383J>
- Cross, A.J., Dunnill, C.W., Parkin, I.P., 2012. Production of predominantly anatase thin films on various grades of steel and other metallic substrates from TiCl₄ and ethyl acetate by atmospheric pressure CVD, *Chem. Vap. Depos.* 18 (4-6), 133-139.
- Djaoued, Y., Badilescu, S., Ashrit, P. V., Bersani, D., Lottici, P.P., Brüning, R., 2002. Low temperature sol-gel preparation of nanocrystalline TiO₂ thin films. *J. Sol-Gel Sci. Technol.* 24, 247–254. <https://doi.org/10.1023/A:1015305328932>
- El-Sherbiny, S., Morsy, F., Samir, M., Fouad, O.A., 2014. Synthesis, characterization and application of TiO₂ nanopowders as special paper coating pigment. *Appl. Nanosci.* 4, 305–313. <https://doi.org/10.1007/s13204-013-0196-y>
- Eriksson, G., Pelton, A.D., 1993. Critical evaluation and optimization of the thermodynamic properties and phase diagrams of the MnO-TiO₂, MgO-TiO₂, FeO-TiO₂, Ti₂O₃-TiO₂, Na₂O-TiO₂, and K₂O-TiO₂ systems. *Metall. Trans. B* 24, 795–805. <https://doi.org/10.1007/BF02663140>
- Etacheri, V., Kuo, Y., Van Der Ven, A., Bartlett, B.M., 2013. Mesoporous TiO₂-B microflowers composed of (110) facet-exposed nanosheets for fast reversible lithium-ion storage. *J. Mater. Chem. A* 1, 12028–12032. <https://doi.org/10.1039/c3ta12920a>
- Fictorie, C.P., Evans, J.F., Gladfelter, W.L., 1994. Kinetic and mechanistic study of the chemical vapor deposition of titanium dioxide thin films using tetrakis-(isopropoxy)-titanium(IV). *J. Vac. Sci. Technol. A Vacuum, Surfaces, Film.* 12, 1108–1113. <https://doi.org/10.1116/1.579173>
- Fukuzumi, Y., Kobayashi, W., Moritomo, Y., 2016. Size dependent ion diffusion in Na₂Ti₃O₇ and Na₂Ti₆O₁₃. *J. Adv. Nanomater.*, 1, 39-49. <https://doi:10.22606/jan.2016.11005>

- Guillén, C., Montero, J., Herrero, J., 2014. Anatase and rutile TiO₂ thin films prepared by reactive DC sputtering at high deposition rates on glass and flexible polyimide substrates. *J. Mater. Sci.* 49, 5035–5042. <https://doi.org/10.1007/s10853-014-8209-0>
- Henkelman, G., Uberuaga, B.P., Jónsson, H., 2000. Climbing image nudged elastic band method for finding saddle points and minimum energy paths. *J. Chem. Phys.* 113, 9901–9904. <https://doi.org/10.1063/1.1329672>
- Huang, C., Zhu, K., Qi, M., Zhuang, Y., Cheng, C., 2012. Preparation and photocatalytic activity of bicrystal phase TiO₂ nanotubes containing TiO₂-B and anatase. *J. Phys. Chem. Solids* 73, 757–761. <https://doi.org/10.1016/j.jpcs.2012.01.018>
- Izquierdo, G., West, A.R., 1980. Phase equilibria in the system Li₂O-TiO₂. *Mater. Res. Bull.* 15, 1655–1660. [https://doi.org/10.1016/0025-5408\(80\)90248-2](https://doi.org/10.1016/0025-5408(80)90248-2)
- Jayasinghe, R.C., Perera, A.G.U., Zhu, H., Zhao, Y., 2012. Optical properties of nanostructured TiO₂ thin films and their application as antireflection coatings on infrared detectors. *Opt. Lett.* 37, 4302. <https://doi.org/10.1364/ol.37.004302>
- Joubert, D., 1999. From ultrasoft pseudopotentials to the projector augmented-wave method. *Phys. Rev. B - Condens. Matter Mater. Phys.* 59, 1758–1775. <https://doi.org/10.1103/PhysRevB.59.1758>
- Kataoka, K., Awaka, J., Kijima, N., Hayakawa, H., Ohshima, K.-i., Akimoto, J., 2011. Ion-Exchange Synthesis, Crystal Structure, and Electrochemical Properties of Li₂Ti₆O₁₃. *Chem. Mater.*, 23, 2344-2352. <https://doi:10.1021/cm103678e>
- Kresse, G., Furthmüller, J., 1996a. Efficient iterative schemes for ab initio total-energy calculations using a plane-wave basis set. *Phys. Rev. B - Condens. Matter Mater. Phys.* 54, 11169–11186. <https://doi.org/10.1103/PhysRevB.54.11169>
- Kresse, G., Furthmüller, J., 1996b. Efficiency of *ab-initio* total energy calculations for metals and semiconductors using a plane-wave basis set. *Comput. Mater. Sci.* 6, 15–50. [https://doi.org/10.1016/0927-0256\(96\)00008-0](https://doi.org/10.1016/0927-0256(96)00008-0)
- Kresse, G., Hafner, J., 1993. Ab initio molecular dynamics for liquid metals. *Phys. Rev. B* 47, 558–561. <https://doi.org/10.1103/PhysRevB.47.558>
- Kuganathan, N., Ganeshalingam, S., Chroneos, A., 2019. Defects, Diffusion, and Dopants in Li₂Ti₆O₁₃: Atomistic Simulation Study. *Materials*, 12, 2851. <https://doi:10.3390/ma12182851>
- Li, W., Liu, C., Zhou, Y., Bai, Y., Feng, X., Yang, Z., Yang Lu, L., Lu, X., Chan, K.Y., 2008. Enhanced photocatalytic activity in anatase/TiO₂ (B) core-shell nanofiber. *J. Phys. Chem. C* 112 (51), 20539-20545. <http://doi.org/10.1021/jp808183q>.
- Liu, N., Chen, X., Zhang, J., Schwank, J.W., 2014. A review on TiO₂-based nanotubes synthesized via hydrothermal method: Formation mechanism, structure modification, and photocatalytic applications. *Catal. Today* 225, 34–51. <https://doi.org/10.1016/j.cattod.2013.10.090>
- Ma, Y., Wang, X., Jia, Y., Chen, X., Han, H., Li, C., 2014. Titanium dioxide-based nanomaterials for photocatalytic fuel generations. *Chem. Rev.* 114, 9987–10043. <https://doi.org/10.1021/cr500008u>
- Malcolm W. Chase, J., 1990. NIST-JANAF Thermochemical Tables, Fourth. ed, Journal of Physical and Chemical Reference Data. American Chemical Society and the American Institute of Physics, New York. <https://doi.org/10.1021/ac00212a751>

- Masuda, Y., Jinbo, Y., Koumoto, K., 2009. Room temperature CVD of TiO₂ thin films and their electronic properties. *Sci. Adv. Mater.* 1, 138–143. <https://doi.org/10.1166/sam.2009.1036>
- Mohamed, M.M., Asghar, B.H.M., Muathen, H.A., 2012. Facile synthesis of mesoporous bicrystallized TiO₂(B)/anatase (rutile) phases as active photocatalysts for nitrate reduction. *Catal. Commun.* 28, 58–63. <https://doi.org/10.1016/j.catcom.2012.08.012>
- Monkhorst, H.J., Pack, J.D., 1976. Special points for Brillouin-zone integrations. *Phys. Rev. B* 13, 5188–5192. <https://doi.org/10.1103/PhysRevB.13.5188>
- Perdew, J.P., Burke, K., Ernzerhof, M., 1996. Generalized gradient approximation made simple. *Phys. Rev. Lett.* 77, 3865–3868. <https://doi.org/10.1103/PhysRevLett.77.3865>
- Pimta, K., Autthawong, T., Yodying, W., Phromma, C., Haruta, M., Kurata, H., Sarakonsri, T., Chimupala, Y., 2023. Development of bronze phase titanium dioxide nanorods for use as fast-charging anode materials in lithium-ion batteries. *ACS Omega.* 17, 15360–15370. <https://doi.org/10.1021/acsomega.3c00618>
- Pyun, M.W., Kim, E.J., Yoo, D.H., Hahn, S.H., 2010. Oblique angle deposition of TiO₂ thin films prepared by electron-beam evaporation. *Appl. Surf. Sci.* 257, 1149–1153. <https://doi.org/10.1016/j.apsusc.2010.08.038>
- Samsudin, E.M., Sze, N.G., Ta, Y.W., Tan, T.L., Abd. Hamid, S.B., Joon, C.J., 2015. Evaluation on the photocatalytic degradation activity of reactive blue 4 using pure anatase nano-TiO₂. *Sains Malaysiana* 44, 1011–1019. <https://doi.org/10.17576/jsm-2015-4407-13>
- Schneider, J., Matsuoka, M., Takeuchi, M., Zhang, J., Horiuchi, Y., Anpo, M., Bahnemann, D.W., 2014. Understanding TiO₂ photocatalysis: Mechanisms and materials. *Chem. Rev.* 114, 9919–9986. <https://doi.org/10.1021/cr5001892>
- Setvin, M., Shi, X., Hulva, J., Simschitz, T., Parkinson, G.S., Schmid, M., Di Valentin, C., Selloni, A., Diebold, U., 2017. Methanol on Anatase TiO₂ (101): Mechanistic insights into photocatalysis. *ACS Catal.* 7, 7081–7091. <https://doi.org/10.1021/acscatal.7b02003>
- Svora, P., Ecorchard, P., Plížingrová, E., Komárková, B., Pawełkowicz, S.S., Murafa, N., Maříková, M., Smržová, D., Wagner, B., Machálková, A., Bezdička, P., 2020. Influence of Inorganic Bases on the Structure of Titanium Dioxide-Based Microsheets. *ACS Omega*, 5, 23703–23717. <https://doi.org/10.1021/acsomega.0c02570>
- Wan, C., Lu, Y., Jin, C., Sun, Q., Li, J., 2015. A Facile low-temperature hydrothermal method to prepare anatase titania/cellulose aerogels with strong photocatalytic activities for rhodamine B and methyl orange degradations. *J. Nanomater.* 2015. <https://doi.org/10.1155/2015/717016>
- Yang, D., Liu, H., Zheng, Z., Yuan, Y., Zhao, J.C., Waclawik, E.R., Ke, X., Zhu, H., 2009. An efficient photocatalyst structure: TiO₂(B) nanofibers with a shell of anatase nanocrystals. *J. Am. Chem. Soc.* 131, 17885–17893. <https://doi.org/10.1021/ja906774k>
- Yu, X., Pan, H., Wan, W., Ma, C., Bai, J., Meng, Q., Ehrlich, S.N., Hu, Y.S., Yang, X.Q., 2013. A size-dependent sodium storage mechanism in Li₄Ti₅O₁₂ investigated by a novel characterization technique combining in situ X-ray diffraction and chemical sodiation. *Nano Lett.* 13, 4721–4727. <https://doi.org/10.1021/nl402263g>

- Yurkinskii, V.P., Firsova, E.G., Proskura, S.A., 2005. Thermal dissociation of sodium hydroxide upon evacuation. *Russ. J. Appl. Chem.* 78, 360–362. <https://doi.org/10.1007/s11167-005-0296-x>
- Zheng, J., Hu, C., Nie, L., Zang, S., Chen, H., Chen, N., Ma, M., Lai, Q., 2023. Electrolyte manipulation enhanced pseudo-capacitive K-storage for TiO₂ anode. *Appl. Surf. Sci.* 611, 155617. <https://doi.org/10.1016/j.apsusc.2022.155617>
- Zheng, Z., Liu, H., Ye, J., Zhao, J., Waclawik, E.R., Zhu, H., 2009. Structure and contribution to photocatalytic activity of the interfaces in nanofibers with mixed anatase and TiO₂(B) phases. *J. Mol. Catal. A Chem.* 316, 75–82. <https://doi.org/10.1016/j.molcata.2009.10.002>

For Table of Contents Use Only,

Ecofriendly Alkali Metal Cations Diffusion Improves Fabrication of Mixed-phase Titania Polymorphs on Fixed Substrate by Chemical Vapor Deposition (CVD) for Photocatalytic Degradation of Azo Dye

Navadecho Chankhunthod,^{a,i,#} Patcharanan Junploy,^{b,#} Suwit Suthirakun,^c Lappawat Ngamwongwan,^c Chitsanupong Phromma,^d Nantawat Ruchusartsawat,^d Adisak Siyasukh,^d Pattama Yanu,^e Pimluck Kijjanapanich,^f Saranphong Yimklan,^g Apinpus Rujiwatra,^g Rik Drummond-Brydson^{h,} and Yothin Chimupala^{d,j,*}*

- a. Department of Physics, Faculty of Science, Khon Kaen University, Khon Kaen, 40002, Thailand.
- b. Department of Chemistry, Faculty of Science and Technology, Chiang Mai Rajabhat University, Chiang Mai, Thailand.
- c. School of Chemistry, Institute of Science, Suranaree University of Technology, Nakhon Ratchasima 30000, Thailand.
- d. Department of Industrial Chemistry, Faculty of Science, Chiang Mai University, Chiang Mai, 50200, Thailand.
- e. Chiang Mai University Demonstration School, Faculty of Education, Chiang Mai University, Chiang Mai 50200, Thailand.
- f. Department of Environmental Engineering, Faculty of Engineering, Chiang Mai University, Chiang Mai 50200, Thailand
- g. Department of Chemistry, Faculty of Science, Chiang Mai University, Chiang Mai, 50200, Thailand.
- h. School of Chemical and Process Engineering, University of Leeds, Leeds, LS2 9JT, United Kingdom.
- i. Institute of Nanomaterials Research and Innovation for Energy (IN-RIE), NANOTECH-KKU RNN on Nanomaterials Research and Innovation for Energy, Khon Kaen University, 40002, Thailand.
- j. Center of Excellence in Materials Science and Technology, Chiang Mai University, Chiang Mai 50200, Thailand.

Co-first Authors

* Co-corresponding Authors

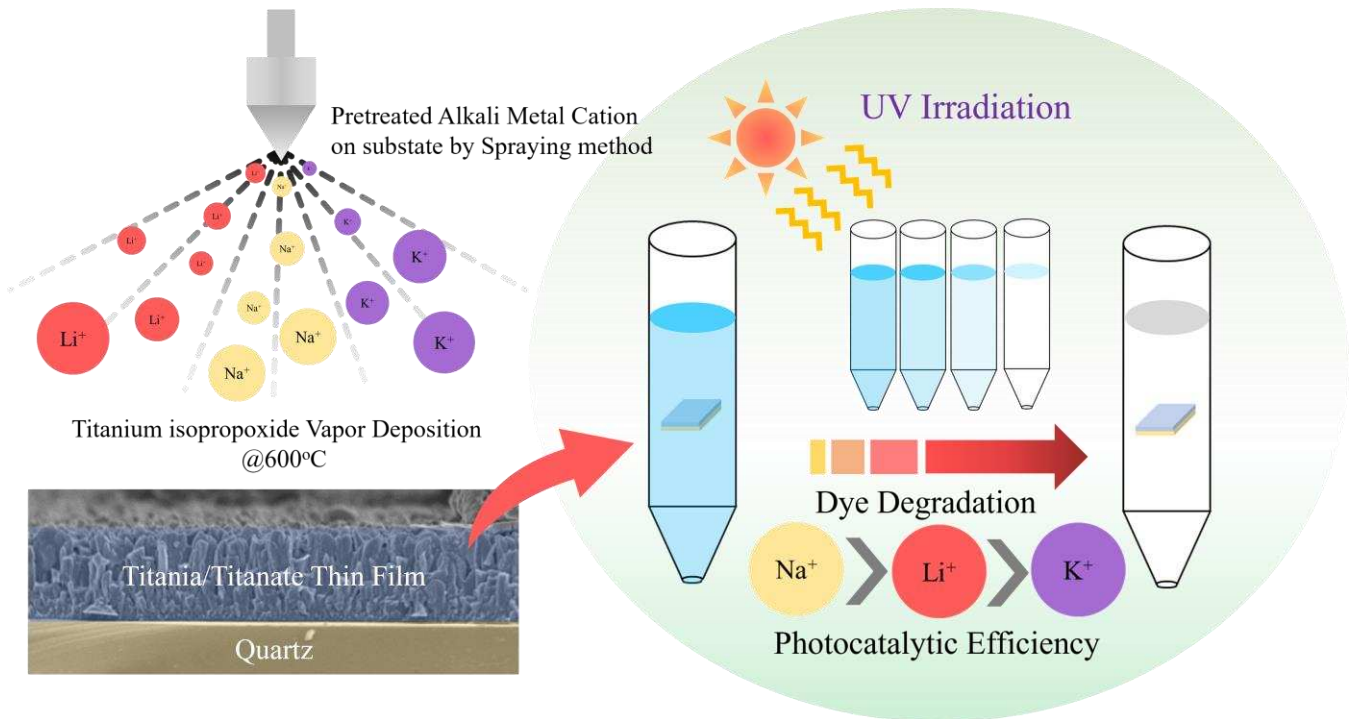
* Email: yothin.chimupala@cmu.ac.th, R.M.Drummond-Brydson@leeds.ac.uk

*To whom the correspondence should be addressed:

Telephone: +66 6259-2469-9

Email Address: yothin.chimupala@cmu.ac.th

Graphical Abstract



Highlight

- The mixed-phase TiO₂/other titania thin films have been synthesized by modified CVD.
- Li⁺, Na⁺, and K⁺ are involved in the modified CVD by pre-treatment onto substrates.
- The different cations promote significantly different phases and compositions of thin films.
- The titania phase formation mechanism was proposed by experimental and DFT calculation.
- The photocatalytic dye degradations of the titania thin-film were studied.